Nanoscale

Accepted Manuscript

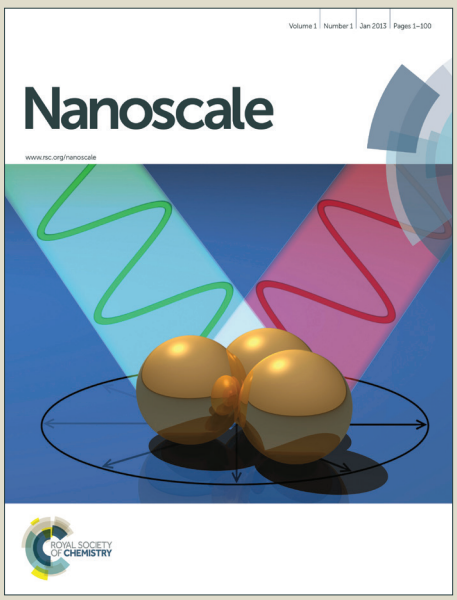

ROYAL SOCIETY OF CHEMISTRY

www.rsc.org/nanoscale

Cite this: DOI: 10.1039/c0xx00000x

www.rsc.org/xxxxxx

ARTICLE TYPE

Controllable copper deficiency in $Cu_{2-x}Se$ nanocrystals with tuning localized surface plasmon resonance and enhancing chemiluminescence†

Shao Qing Lie[a], Dong Mei Wang*[a], Ming Xuan Gao[a], and Cheng Zhi Huang*[ab]

Received (in XXX, XXX) Xth XXXXXXXXX 20XX, Accepted Xth XXXXXXXXX 20XX

DOI: 10.1039/b000000x

Copper chalcogenide nanocrystals (CuCNCs) as a type of semiconductor acting as efficient catalysts have been rarely involved. Herein we report that water-soluble size-controlled $Cu_{2-x}Se$ nanocrystals (NCs), which are copper deficient and could be prepared by redox reaction with the assistance of surfactants, were found to have strong near-infrared localized surface plasmon resonance (LSPR) properties originated from the holes in the valence band, and catalytic activity of more than 500-fold enhancement of the chemiluminescence (CL) in luminol-H_2O_2 system. Mechanism investigations showed that the high concentration of free carriers in $Cu_{2-x}Se$ NCs, derived from high copper deficiencies which make $Cu_{2-x}Se$ NCs be both good electron donor and acceptor with high ionic mobility, could greatly enhance the catalytic ability of $Cu_{2-x}Se$ NCs to facilitate electron-transfer process and decomposition of H_2O_2 into $OH\cdot$ and $O_2^{\cdot-}$, the commonly accepted key intermediates in luminol CL enhancement. So it is concluded that controllable copper deficiencies that are correlated with their near-infrared LSPR are critically responsible for the effective catalysis of $Cu_{2-x}Se$ NCs in the enhanced CL.

Introduction

As an important family of semiconductor nanomaterials, CuCNCs have been attractive recently due to their specific optical[1-4] and optoelectronic properties.[5-7] For example, copper selenide NCs have been intensively studied and widely used in solar cell,[8] optical filter,[9] and super ionic conductors[10] due to their various phases and structural forms, such as stoichiometric Cu_2Se, Cu_3Se_2, CuSe, and $CuSe_2$ NCs, as well as non-stoichiometric $Cu_{2-x}Se$ NCs.[11-13] As a *p*-type semiconductor with electron-ionic conductivity and a direct/indirect band gap of 2.2/1.4 eV,[14] the non-stoichiometric $Cu_{2-x}Se$ NCs are particularly suitable for solar light-sensitive photocatalysts.[15]

Up-to-date investigations focus on the strong near-infrared (NIR) absorption of the cation-deficient $Cu_{2-x}Se$ NCs, proving that the LSPR originates from the high density of holes in the valence band.[16-18] Different from that of noble metal NCs,[19-21] the NIR-LSPR of $Cu_{2-x}Se$ NCs can be easily engineered by changing the materials' composition, temperature, or phase transitions,[22] which can then supply new opportunities for sensing,[23] imaging,[24, 25] photothermal therapy,[26, 27] and plasmonic solar cells.[28, 29] Thus, a lot of efforts have been devoted to achieving fine-tunability in the LSPR properties of CuCNCs,[14, 30-33] providing us with both high fundamental view and technological potential to know more about the NIR-LSPR of $Cu_{2-x}Se$ NCs.

It is well known that defects such as oxygen vacancies and step edges, which have been proposed to participate in chemical catalytic reactions,[34, 35] are the most reactive sites on the surfaces of metal oxides since the defects can bind adsorbates more strongly than normal sites and assist in their dissociation. For example, oxygen vacancies are involved in electrochemical oxygen reduction reactions as their charged nature may control band-bending and thus electron-hole pair separation, greatly enhancing the electrocatalytic activity.[35, 36] As the analogy, copper deficiency in $Cu_{2-x}Se$ NCs is important for arising the plasmon resonance as well as for some electrical properties,[32, 37] but few reports have been involved in the applications of such vacancies for catalysis. Therefore in this contribution, we investigated the $Cu_{2-x}Se$ NCs involved in catalysis chemistry, by taking the example of luminol chemiluminescence (CL), which is simple but can supply us new train of thought for the theoretical understanding of the vacancy and make us find more practical applications such as bioimaging and immunoassay.

In this respect, we developed a new controllable preparation route of Cu_2Se NCs at room temperature by making use of the reaction of selenium nanoparticles acting as a template[38] with copper sulfate solution, and found that the available copper deficient $Cu_{2-x}Se$ NCs can induce more than 500-fold CL enhancement in the typical luminol-H_2O_2 system. The observed enhancement effect is unusual and better than most of the reported NCs,[39] which, as we identified herein, is closely related to the unique electronic structure since the copper deficiency in $Cu_{2-x}Se$ NCs supports markedly an increase of free carrier concentration and mobility, which facilitate the electron-transfer process from luminol to H_2O_2 and accelerate efficiently the decomposition of H_2O_2 to form the active oxygen-related radicals, $OH\cdot$ and $O_2^{\cdot-}$. These active radicals have been commonly identified to be the key intermediates that induced CL enhancement.[40] This investigation could be valuable to obtain new insight into the unique structure characteristics of $Cu_{2-x}Se$ NCs, and broaden the application of the novel semiconductor materials in the fields, such as sensing, catalysis, and solar cell.

Experimental

Apparatus

The UV-vis absorption spectra were measured with a U-3600 spectrophotometer (Hitachi Ltd., Tokyo, Japan). Scanning electron microscopy (SEM) and Transmission electron microscopy (TEM) images were captured using an S-4800 scan electron microscopy (Hitachi, Japan) and transmission electron microscopy (TEM) (JEM-2100, Japan). Elemental analysis was made on ESCALAB 250 X-ray photoelectron spectrometer (Tyoto, Japan). Powder X-ray diffraction (XRD) patterns were obtained using a Shimadzu XRD-7000 and filtered Cu-Ka radiation. Zeta potential and the average hydrodynamic diameters of $Cu_{2-x}Se$ NCs were measured by dynamic laser light scattering (DLS, ZEN3600, Malvern). The ratios of Cu/Se in the nanocrystals and the mass concentration of $Cu_{2-x}Se$ NCs were obtained by using inductively couple plasma atomic emission spectrometry (ICPAES).

Reagents and materials

Luminol, polyvinylpyrrolidone powder (PVP, MW 55 kD) were commercially obtained from Sigma-Aldrich Co. LLC. (USA). Cetyltrimethyl ammonium bromide (CTAB), sodium dodecyl sulfate (SDS) and copper sulfate ($CuSO_4 \cdot 5H_2O$, 99%) were purchased from Sinopharm Chemical Reagent Co. Ltd. (Shanghai, China). Selenious dioxide (SeO_2, 99.9%) was obtained from Aladdin Chemistry Co. Ltd. (Shanghai, China). Polystyrene sulfonate (PSS, MW 70 kD) and vitamin C (Vc) were purchased from Alfa Aesar Co. Ltd. (MA, USA). All chemicals were used as received without further purification and dissolved in doubly distilled water (18.2 MΩ).

Synthesis of $Cu_{2-x}Se$ NCs

1.6 ml 10 mg/ml PSS and 5.5 ml water were added to a round-bottom flask and then it was added 0.1 ml 0.2 M SeO_2 and 0.3 ml 0.4 M Vc, successively. After 10 min, a mixed solution of 0.1 ml 0.4 M $CuSO_4 \cdot 5H_2O$ and 0.4 ml 0.4 M Vc were added under vigorous stirring, in which Vc reduce Cu^{2+} to be Cu^{+}. The resulting mixture was allowed to proceed under vigorous stirring at 30 °C until a green solution was obtained in 10 h, indicating that PSS stablized $Cu_{2-x}Se$ NCs has produced. The yielding products were purified through a 10 kDa dialysis membrane for 1 day with 6 changes of distilled water in order to remove the small molecules and centrifugation if necessary to remove the large molecules. The products were finally stored in a 4 ◦C refrigerator. It is found that the yielding products are stable within 1 month (Fig. S1, ESI†). Other surfactants stabilized $Cu_{2-x}Se$ NCs were synthesized also following the same procedures, but the reaction time is 3 h for CTAB, 10 h for SDS or PVP, respectively. The molar extinction coefficient of all $Cu_{2-x}Se$ NCs were calculated on the absorbance at peak wavelength with various concentrations.[26]

Chemiluminescent measurements

The CL spectra and the dynamic CL intensity-time profiles of PSS-$Cu_{2-x}Se$ NCs-enhanced luminol CL were measured with an ultra-weak BPCL luminescence analyzer (Institute of Biophysics, Chinese Academy of Sciences, Beijing, China) using the static model in a 3-mL quartz cuvette. Before the CL signals were recorded, the analyzer was firstly run for half an hour every time for the purpose of good reproducibility. The dynamic profiles were displayed and integrated for a 0.2 s interval at -750 V. The CL spectra were obtained through a series of high-energy cutoff filters (wavelengths from 230 to 640 nm), which were placed between the flow CL cell and the photomultiplier of the analyzer. 250 μL of luminol solution was quickly injected by a microliter syringe into a mixture premixed with 100 μL of H_2O_2 and 100 μL of PSS-$Cu_{2-x}Se$ NCs in the cuvette. When investigating the influence of different radical scavengers on luminol-H_2O_2 CL in the presence of $Cu_{2-x}Se$ NCs, 100 μL of radical scavengers with different concentrations were first introduced into the mixture of H_2O_2 and $Cu_{2-x}Se$ NCs following the same experimental procedures as described above. $(I_0 - I)/I_0 \times 100\%$ was used to calculate CL percent inhibition, and the I_0 or I were the CL intensities in the absence or presence of radical scavengers, respectively.

Results and discussion

A route to prepare $Cu_{2-x}Se$ NCs with controllable size

Template-directed synthesis has been identified as an effective and facile strategy to prepare CuCNCs.[38, 41-43] Although this approach usually requires at relatively low temperature or even if at room temperature, the as-prepared CuCNCs have weak LSPR absorption. Considering that surfactants can influence both the morphology of $Cu_{2-x}Se$ NCs related to the LSPR frequency[32] and the catalytic activity of NCs,[44, 45] we herein developed a template-directed synthesis route to prepare $Cu_{2-x}Se$ NCs with controllable size by introducing four kinds of water-soluble surfactants including cations (CTAB), anions (SDS), anionic polymer (PSS), non-ionic polymer (PVP).

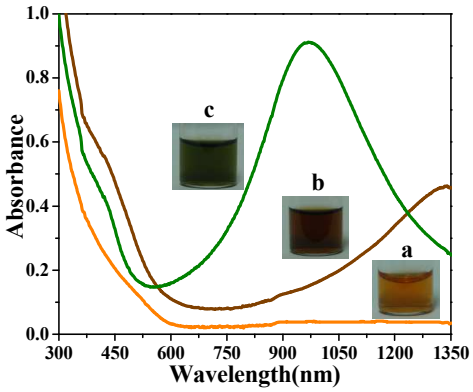

Fig.1 Step-by-step absorption spectra and visual observation of the formation of $Cu_{2-x}Se$ NCs stablized by PSS. (a) The Se NCs obtained with the reaction of Vc and SeO_2 in 10 min in the first step. (b) The Cu_2Se NCs obtained after cuprous ion got mixed with Se NCs in 0.5 h in the second step. (c) The $Cu_{2-x}Se$ NCs obtained with extended reaction time of Cu_2Se NCs being oxidized in the third step.

The built-up simple reaction route was composed of three steps (Fig. 1). At first, Vc was employed to reduce SeO_2 into orange Se NCs (Fig. 1a) in the presence of surfactants. Secondly, Cu_2Se NCs were formed with the addition of Cu^{+} (mixture solution of $CuSO_4$ and Vc) into Se NCs since Cu^{+} can catalyze Se^0 into Se^{2-} and Se^{4+},[38] during which the colour of solution

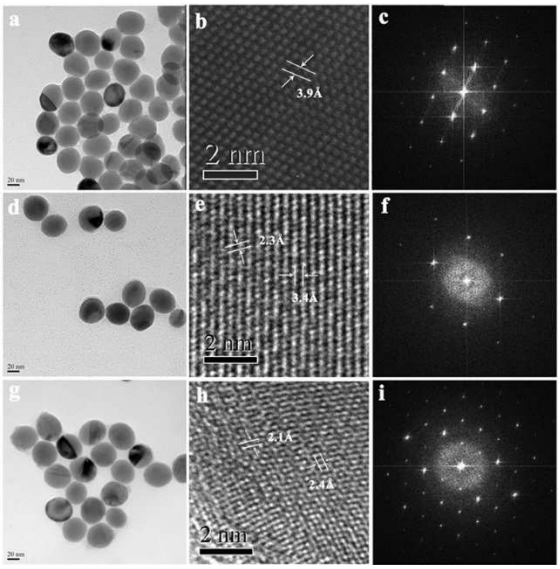

Fig.2 TEM images to visualize the formation of Se NCs, Cu_2Se NCs and $Cu_{2-x}Se$ NCs stablized by PSS. TEM images (a, d, g), HR-TEM images (b, e, h), and corresponding numerical diffractogram (FFTs, c, f, i) of Se NCs (a, b, c), Cu_2Se NCs (d, e, f), and $Cu_{2-x}Se$ NCs (g, h, i), respectively.

changed from orange to brown (Fig. 1b). Finally, the as-formed Cu_2Se NCs gradually transformed into $Cu_{2-x}Se$ NCs with the colour change to green through a phase transformation process promoted by air exposure and oxidants unreacted (Fig. 1c).[10] The formation of the orange Se NCs in the first step could be identified by TEM and HR-TEM images (Fig. 2a, b, c), and these Se NCs had a spacing of 0.39 nm corresponding to (100) planes.[46] Fig. 2 also clearly showed the formation of Cu_2Se NCs and $Cu_{2-x}Se$ NCs, wherein HR-TEM images demonstrated the phase transformation from Cu_2Se NCs with the measured spacings of 3.4 Å and 2.3 Å corresponding to the (060) and (090) plans to $Cu_{2-x}Se$ NCs with the measured spacings of 2.4 Å and 2.1 Å corresponding to the (012) and (220) plans.[10, 47]

As TEM images in Fig. 3 showed, the as-prepared particles after the three steps were quite monodispersed and uniform, and their size could be adjusted ranging from 14.5 nm to 52.0 nm by changing surfactants. Powder X-ray diffraction (XRD) identified that the as-prepared $Cu_{2-x}Se$ NCs were cubic berzelianite phase with well-defined crystalline (Fig. S2, ESI†), while the X-ray photoelectron spectroscopic (XPS) measurements (Fig. S3, ESI†) also identified the $Cu_{2-x}Se$ phase with the binding energies of 932.30 eV for Cu $2p_{3/2}$ and 54.84 eV for Se 3d. The Cu $2p_{3/2}$ peak appearing at 932.30 eV corresponded to either Cu^0 or Cu (I). A noticeable phenomenon is that asymmetric peak shape toward high binding energies appeared, indicating the presence of Cu(II).[48] In other words, the available final products were nonstoichiometric $Cu_{2-x}Se$ with high copper deficiency.[49]

The monodispersed growth of $Cu_{2-x}Se$ NCs with size tunability should be attributed to the surfactant and the size-focusing effect[32] as the size of the nanoparticles could be restricted to a certain range with changing concentration of different surfactants (Fig. S4, ESI†). Therefore, it is suggested that surfactants may complex somehow selenium and then copper ions in the reaction.

In the first step, the type of the surfactants may be essential in

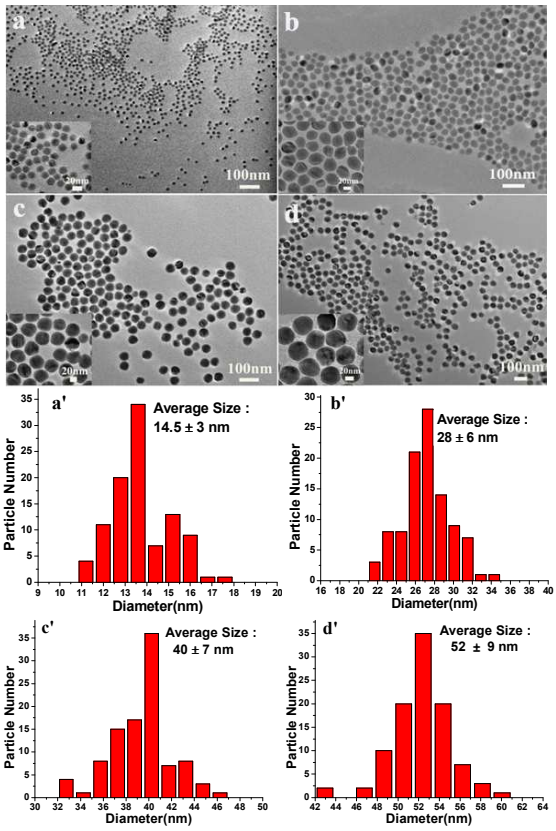

Fig.3 Surfactant-dependent sizes of $Cu_{2-x}Se$ NCs as shown by TEM images. $Cu_{2-x}Se$ NCs were coated by CTAB (a, a'), SDS (b, b'), PSS (c, c') and PVP (d, d'), respectively. Size distributions are obtained by counting 100 particles of each sample.

the synthesis of monodispersed size-tunable Se NCs (Table.S1, ESI†). During the formation of Se NCs, the size of Se NCs is controlled by surfactants following a burst of nucleation having a constant volumetric growth rate.[32] CTAB and SDS are molecules highly smaller than PVP or PSS, thus allowing for a larger mobility and reactivity of the surfactant-ion system. This could also decrease the barrier for nucleation favoring, in the case of CTAB- and SDS-complexed ions, many more nuclei, smaller growing. Furthermore, there should be considered the fact that PVP and PSS are polymeric molecules, therefore offering many anchoring groups to selenium with respect to CTAB or SDS. Therefore, the size of Se NCs obtained by CTAB or SDS is observed to be relatively smaller than that by PSS or PVP.

In the second step, during which cuprous ion react with the templated Se NCs,[50] the formation of Cu_2Se may be controlled by different rates of ionic diffusion induced by different surfactants. The oxygen groups in SDS or PSS or PVP surfactant have a trend to coordinate to cuprous cations, which slow down the diffusion to the nucleation,[51] so the formation rates of product prepared by different surfactants are different but do not induce large change of size from Se NCs to Cu_2Se NCs as shown by TEM image (Fig. 2) and the DLS measurement (Table.S1, ESI†).

In the third step, the phase transformation from Cu_2Se to $Cu_{2-x}Se$ is observed by the colour change and the strong absorption in NIR (Fig 1c), where air exposure has produced an oxidation of the nanoparticle surface which also be supported by the XRD pattern (Fig. S5, ESI†),[49] then the creation of a potential along the particle diameter which has promoted a diffusion of copper ions

from the inner core to the surface. It is found that the NCs preserve their size and shape in the transformation (Fig. 2), which is similar to the reported chemical transformation starting from Cu_2Se nanocrystals.[10, 47]

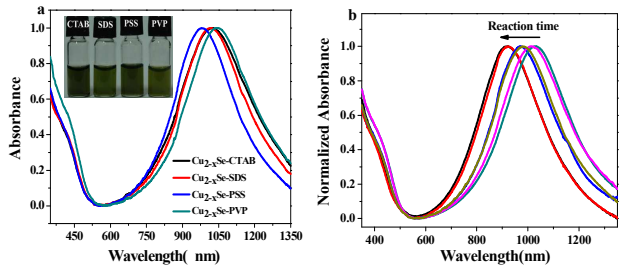

Fig.4 NIR-LSPR absorption spectra of $Cu_{2-x}Se$ NCs. (a) The absorption spectra of crystalline $Cu_{2-x}Se$ NCs coated by CTAB (30 °C, 3 h), SDS (30 °C, 10 h), PSS (30 °C, 10 h), PVP (30 °C, 10 h) with the size of 14.5 nm, 28 nm, 40 nm and 52 nm, respectively. Different surfactants capping $Cu_{2-x}Se$ NCs showed different absorption band characterized at 1025 nm, 1020 nm, 980 nm, 1040 nm with the molar extinction coefficient of 3.8×10^8 $M^{-1}cm^{-1}$, 2.2×10^9 $M^{-1}cm^{-1}$, 4.7×10^9 $M^{-1}cm^{-1}$, 1.2×10^{10} $M^{-1}cm^{-1}$, respectively. (b) With reaction time going from 8 h to 12 h at 30 °C, the absorption spectra of crystalline PSS-$Cu_{2-x}Se$ are blue-shifted.

High copper deficiency of $Cu_{2-x}Se$ NCs

The available nonstoichiometric $Cu_{2-x}Se$ NCs with high copper deficiency could be well-dispersed in water, and has absorption from UV to NIR region (Fig. 4a). The absorption in the UV-VIS region below 500 nm has been ascribed to the direct band gap, and the one in NIR region should be the LSPR.[4, 7, 26] It has been known that the NIR-LSPR depends on the relatively high carrier (holes) concentration and sizes of nanocrystals.[22, 32] Here the NIR-LSPR is easily tuned by changing the surfactants and reaction time (Fig. 4b). Within the same reaction time, different surfactants such as PVP, SDS and PSS can be used to control the LSPR frequency of $Cu_{2-x}Se$ NCs, which have strong absorption peak centered at 1045 nm, 1020 nm and 980 nm. In addition, the LSPR frequency of $Cu_{2-x}Se$ NCs weakly depends on the size but rely more on the electric charge of surfactants. As the electric charge of surfactants are more negative (Table. S1, ESI†), $Cu_{2-x}Se$ NCs show a more significant blue-shift in LSPR absorption with a Cu/Se ratio of 1.6 (x=0.4).

It was also found that CTAB could accelerate the phase transformation from the Cu_2Se NCs to the $Cu_{2-x}Se$ NCs with a Cu/Se ratio of 1.2 (x=0.8) within 3 h. Compared with other surfactants, CTAB can make $Cu_{2-x}Se$ NCs have a highest copper deficiency, but can not unexpectedly make any blue shift in LSPR of $Cu_{2-x}Se$ NCs,[17] which should be ascribed to the more positive charge of CTAB than others. Therefore it is suggested that positive charge on the surface of $Cu_{2-x}Se$ NCs may trap free holes and thereby reduce the effective free carrier concentration, which is similar to oleic acid as a Lewis acid having ability to accept electrons.[32] On the contrary, the negative charge on the surface of $Cu_{2-x}Se$ NCs highly increased the charge carrier density, which leads to a blue-shift of LSPR. Besides, the molar extinction coefficient of $Cu_{2-x}Se$ NCs show strong size dependence as the size increase the molar extinction coefficient get increased.

Furthermore, it is easy to control the NIR-LSPR band of $Cu_{2-x}Se$ NCs by extending the reaction time in the presence of PSS (Fig. 4b), and thus we can adjust the copper deficiency of $Cu_{2-x}Se$ NCs since the blue shift of NIR-LSPR indicates increasing copper deficiency,[17, 47] and thus the copper deficiency is controllable. Additonally, the LSPR features induced by the copper deficiency of the available $Cu_{2-x}Se$ NCs are greatly dependent on the surrounding medium, and it is found that the NIR absorption of $Cu_{2-x}Se$ NCs gets red-shifted with increasing refractive index of the surrounding solvent media (Fig. S6, ESI†), identical to the LSPR absorption features of noble metal nanocrystals such as gold and silver nanocrystals.[21, 52]

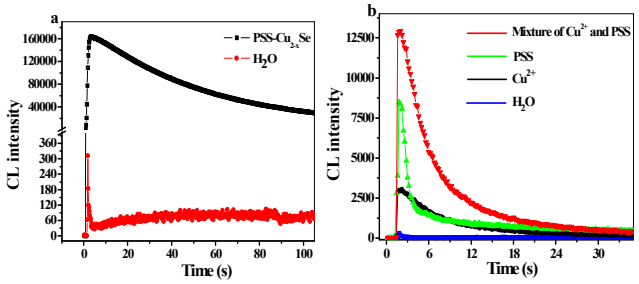

Fig.5 $Cu_{2-x}Se$ NCs with high copper deficiency (x~0.4) induced strong chemiluminescence. Kinetic monitoring on luminol-H_2O_2 CL in the presence of (a) PSS-$Cu_{2-x}Se$ NCs and (b) the reagents including Cu^{2+}, PSS, or their mixture used in the synthesis processes. Conditions: luminol, 2.0×10^{-4} M; H_2O_2, 22.2 μM; PSS-$Cu_{2-x}Se$ NCs, 70.0 pM; Cu^{2+}, 5 mM; PSS, 2.0 mg / mL.

Copper deficiency of $Cu_{2-x}Se$ NCs induced strong CL enhancement

In order to identify the excellent catalytic ability is related to the high copper deficiency of $Cu_{2-x}Se$ NCs, we take the well-known luminol-H_2O_2 CL system as an example. Fig. 5 shows the highly catalytic performance of $Cu_{2-x}Se$ NCs coated by PSS (PSS-$Cu_{2-x}Se$ NCs), in comparison with the dynamic CL intensity-time profiles of luminol-H_2O_2 system in the absence and presence of PSS-$Cu_{2-x}Se$ NCs. It can be seen that PSS-$Cu_{2-x}Se$ NCs can greatly enhance the CL intensity of luminol as high as up to 530 times, compared to the weak luminol CL oxidized only by H_2O_2 in alkaline medium (Fig. 5a). This strongly enhanced CL effect is the best one among the reported nanocatalysis.[33] Similar to other nanocatalysts, the catalytic activity of PSS-$Cu_{2-x}Se$ NCs is closely related to the pH and the concentrations of reaction reagents. The optimal condition was 2.0×10^{-4} M luminol in NaOH solution (pH 11.1), 70.0 pM PSS-$Cu_{2-x}Se$ NCs and 22.2 μM H_2O_2, respectively (Fig. S7, ESI†).

In such case, it is necessary to clarify whether the observed catalytic effect of PSS-$Cu_{2-x}Se$ NCs is derived from the unreacted reagents used in the synthetic processes. Fig. 5b shows that there are really some degree of CL enhancement by Cu^{2+}, PSS, or the mixture of Cu^{2+} and PSS solutions with the same concentrations as the synthetic procedures, but the enhanced degrees are greatly weaker than that of PSS-$Cu_{2-x}Se$ NCs under the same conditions. Furthermore, the as-prepared PSS-$Cu_{2-x}Se$ NCs have been subjected to dialysis (24 h) and centrifugation (10000 rpm, 10 min) to remove the residual Cu^{2+} or PSS species. Hence, the

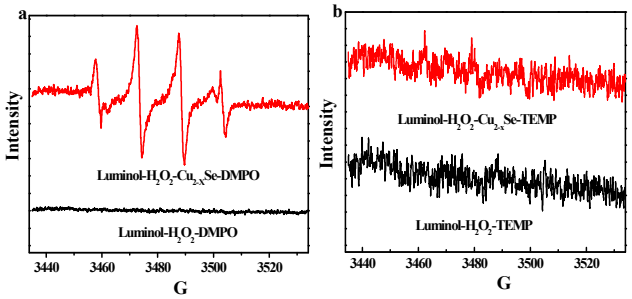

Fig.6 ESR spectra of (a) DMPO-OH· adduct, and (b) nitroxide radicals generated by the reaction of TEMP probe with $^1O_2$ in luminol-H_2O_2 system in the presence (red line) or absence (black line) of PSS-$Cu_{2-x}Se$. Conditions: modulation amplitude, 1.944 G; microwave power, 1.002e + 001 mW; receiver gain, 1.00e + 005; sweep width, 100.00 G. The ESR measurements were achieved with a Bruker ESP-300E spectrometer operating in the X-band at room temperature.

possibility of the CL enhancement effect from concomitant species such as Cu^{2+} or PSS can be excluded, and really from the intrinsic catalytic property of the intact PSS-$Cu_{2-x}Se$ NCs.

The CL spectra of luminol-H_2O_2 either in the presence orabsence of PSS-$Cu_{2-x}Se$ NCs were acquired (Fig. S8, ESI†). It was clearly indicated that the maximum emission was ~440 nm, revealing that the luminophors in both cases are the excited-state 3-aminophthalate anions (3-APA*), in agreement with the reported nanocatalysis.[32, 53, 54] In addition, the measurements of SEM and TEM (Fig. S9, ESI†) showed no significant differences or changes in the size, and shape for PSS-$Cu_{2-x}Se$ NCs before or after the CL reaction, so we can conclude that the NCs act as a catalyst to enhance luminol CL.

In order to identify the catalytic process of PSS-$Cu_{2-x}Se$ NCs during the CL process, further investigations are necessary in terms of the key oxygen-related radical intermediates induced luminescence enhancement, such as quenching experiments of different active oxygen radical scavengers on the CL intensity. Therefore, the effects of Vc (a common scavenger of oxygen-related radicals), thiourea (a scavenger of OH· radical), superoxide dismutase (SOD, a scavenger of $O_2^{\cdot-}$ radical) or NaN_3 (a scavenger of $^1O_2$) were measured. The results indicated that Vc, thiourea and SOD all decreased the CL remarkably, but no CL inhibition occurred for NaN_3 (Fig. S10, ESI†), suggesting that it were that OH· and $O_2^{\cdot-}$, not $^1O_2$, were produced during the CL process. In other words, OH· and $O_2^{\cdot-}$ did contribute to the observed CL. Apart from the breakdown of H_2O_2, a small fraction of above radicals could come from dissolved oxygen of the reagent solutions, because there were some changes in average CL intensity CL signal (less than 20% changes) when N_2 was bubbled into the reactant solutions for a few minutes before the CL reaction.

Furthermore, room temperature electron spin resonance (ESR) technique, which was used to detect oxygen-related radicals because of their short lifetime, was explored, wherein 5, 5-Dimethyl-1-pyrroline N-oxide (DMPO) was used as a specific target molecule to determine OH·. As Fig. 6a shows, the DMPO / OH· adduct signal intensity of ESR spectra in the presence of PSS-$Cu_{2-x}Se$ NCs is clear and much stronger than that without NCs, indicating that PSS-$Cu_{2-x}Se$ NCs have excellent catalytic activity to accelerate the decomposition of H_2O_2 to generate a high yield of OH· on their surface. As a specific target molecule

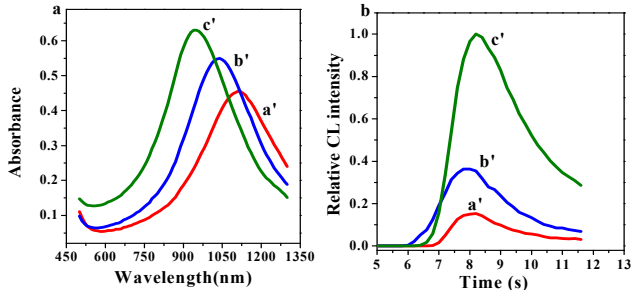

Fig.7 The PSS-$Cu_{2-x}Se$ NCs with different free carrier concentrations and their kinetic monitoring on luminol-H_2O_2 CL. (a) Three PSS-$Cu_{2-x}Se$ NCs (a', b' and c') with different absorption spectra were obtained in different reaction time. (b) Kinetic monitoring on luminol-H_2O_2 CL in the presence of a', b' and c', respectively. Conditions: luminol, 2.0×10^{-4} M; H_2O_2, 1×10^{-4} M.

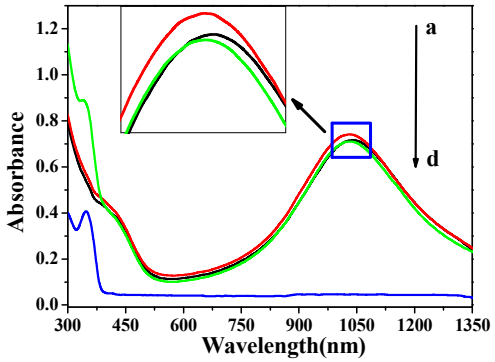

Fig.8 UV-visible absorption spectra of (a) H_2O_2-PSS-$Cu_{2-x}Se$, (b) PSS-$Cu_{2-x}Se$, (c) luminol-H_2O_2-PSS-$Cu_{2-x}Se$, and (d) luminol-H_2O_2. Final concentrations: luminol, 2.0×10^{-4} M; H_2O_2, 222 μM.

of $^1O_2$, 2, 2, 6, 6-tetramethyl-4-piperidine (TEMP) can react with $^1O_2$ to form a stable, ESR measurable 2,2,6,6-tetramethyl-4-piperidine-N-oxide (TEMPO) adduct. However, regardless of the presence or absence of NCs, the signal intensity of TEMPO remains nearly the same in luminol-H_2O_2 system (Fig. 6b), testifing no generation of $^1O_2$, identical to the results of the above quenching experiments. In fact, $Cu_{2-x}Se$ NCs coated by the other three surfactants (SDS, PVP, and CTAB) can also enhance the CL at least 500 times (Fig. S11, ESI†). Moreover, it is found that $Cu_{2-x}Se$ NCs (x~0) can not strongly induce an enhancement of CL compared to $Cu_{2-x}Se$ NCs (x>0) (Fig. S12, ESI†). Therefore, the unique structures of $Cu_{2-x}Se$ NCs, especially the high copper deficiencies, play a critical role in their excellent catalytic activity. As Fig. 7 displayed, $Cu_{2-x}Se$ NCs with increasing density of free carriers (holes) induced by copper deficiency show the increase of catalytic activity. It has been reported that vacancies in the structure would make charge carrier density increase, and thus enhance electronic properties.[10] Similarly, copper deficiency in $Cu_{2-x}Se$ NCs should be responsible for the increase of charge carrier density which may really induce an enhancement of the catalytic activity on luminol-H_2O_2 CL system.

On the other hand, we tested the spectral changes of $Cu_{2-x}Se$ NCs before and after luminol CL (Fig. 8). As expected, at the beginning, a blue shift of the LSPR peak was observed for $Cu_{2-x}Se$ NCs after the addition of H_2O_2, due to the fact that electron transfer occurred from NCs to H_2O_2 which conferred a decrease in electron density of NCs. Then, when luminol was added to the mixture of NCs and H_2O_2, the characteristic LSPR peak of NCs

showed some recovery to the original position, revealing that electrons from luminol were somehow re-injected into NCs. These novel observations confirmed NCs being good electron donor and acceptor could facilitate not only the breakdown H_2O_2 to produce oxygen-related radicals, but also electron-transfer processes taking place on the NC surface, similar to the previously reported nanocatalysis.[40] As shown in scheme 1, the mechanism clearly demonstrates the importance of copper deficiency in making $Cu_{2-x}Se$ NCs facilitate electron-transfer from luminol to H_2O_2 and the decomposition of H_2O_2 into $OH\cdot$ and $O_2\cdot^-$.

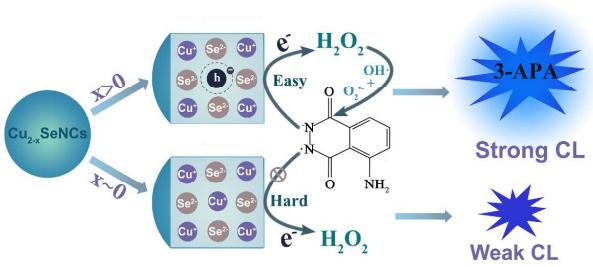

Scheme 1. Illustration of the high performence of $Cu_{2-x}Se$ NCs for luminol-H_2O_2 CL system.

Besides, the possibility that copper ion as a catalyst to decompose H_2O_2 into $OH\cdot$ and $O_2\cdot^-$ in alkaline medium[55] should be considered. As our experiment had demonstrated the existence of $OH\cdot$ and $O_2\cdot^-$ that contribute to the observed strong CL by oxidizing the luminol to be 3-APA*, we supposed that the copper ion on the surface of $Cu_{2-x}Se$ NCs had an important role on increasing the CL signal of luminol-H_2O_2 system. However, with the same copper ion concentration, $Cu_{2-x}Se$ NCs had stronger catalytic ability than that of the free copper ion (Fig. 5). Moreover, the higher free carrier concentrations have $Cu_{2-x}Se$ NCs, the stronger the CL signal show $Cu_{2-x}Se$ NCs (Fig. 7). Therefore, it is not only the copper ion but copper deficiency that play prominent part in CL enhancement. The copper deficiency in $Cu_{2-x}Se$ NCs is responsible for the formation of hole, high free carrier concentration and high ionic mobility, which then largely prompts the catalytic ability of $Cu_{2-x}Se$ NCs to decompose H_2O_2 and facilitate the electron-transfer processes.

Conclusions

In summary, we developed a simple method to synthesize $Cu_{2-x}Se$ NCs with different surfactants, wherein the surfactants in the reaction of cuprous and Se NCs not only control the size of $Cu_{2-x}Se$ NCs but also confine carrier (holes) to a certain concentration. Owing to the controllable copper deficiencies, the as-prepared $Cu_{2-x}Se$ NCs have strong NIR-LSPR properties, and excellent catalytic activity of more than 500-fold CL enhancement in luminol-H_2O_2 system mainly through the commonly accepted $OH\cdot$ and $O_2\cdot^-$. The present study displays a new application of $Cu_{2-x}Se$ NCs in CL field, which should be important for gaining a better understanding of the unique structure of copper deficiencies, and further research about the proposed NCs is now in progress.

Acknowledgements

The presented research was financially supported by the National Natural Science Foundation of China (NSFC, 21375109) and the Cultivation Plan of Chongqing Science & Technology Commission for 100 Outstanding Science and Technology Leading Talents.

Notes and references

[a] *Key Laboratory of Luminescence and Real-Time Analytical Chemistry (Southwest University), Ministry of Education, College of Chemistry and Chemical Engineering, Southwest University, Chongqing, 400715, P. R. China. E-mail: wangdm@swu.edu.cn, and chengzhi@swu.edu.cn, Tel: (+86) 23 68254659, Fax: (+86) 23 68367257.*

[b] *College of Pharmaceutical Science, Southwest University, Chongqing 400716, China*

† Electronic Supplementary Information (ESI) available: Experimental section and additional figures for XRD, XPS, UV absorption, chemiluminescent spectra, SEM and TEM images. See DOI: 10.1039/b000000x/

1 A. M. Malyarevich, K. V. Yumashev, N. N. Posnov, V. P. Mikhailov, V. S. Gurin, V. B. Prokopenko, A. A. Alexeenko and I. M. Melnichenko, *J. Appl. Phys.*, 2000, **87**, 5.
2 Y. Xie, L. Carbone, C. Nobile, V. Grillo, S. D'Agostino, F. Della Sala, C. Giannini, D. Altamura, C. Oelsner, C. Kryschi and P. D. Cozzoli, *ACS Nano*, 2013, **7**, 7352-7369.
3 I. Kriegel, J. Rodriguez-Fernandez, A. Wisnet, H. Zhang, C. Waurisch, A. Eychmuller, A. Dubavik, A. O. Govorov and J. Feldmann, *ACS Nano*, 2013, **7**, 4367-4377.
4 A. L. Routzahn, S. L. White, L.-K. Fong and P. K. Jain, *Isr. J. Chem.*, 2012, **52**, 983-991.
5 J. J. Loferski, *Mater. Sci. Eng., B*, 1992, **13**, 271-277.
6 J. Choi, N. Kang, H. Y. Yang, H. J. Kim and S. U. Son, *Chem. Mater.*, 2010, **22**, 3586-3588.
7 F. Scotognella, G. Valle, A. Srimath Kandada, M. Zavelani-Rossi, S. Longhi, G. Lanzani and F. Tassone, *Eur. Phys. J. B*, 2013, **86**, 1-13.
8 R. S. Mane, S. P. Kajve, C. D. Lokhande and S.-H. Han, *Vacuum*, 2006, **80**, 631-635.
9 S. T. Lakshmikumar and A. C. Rastogi, *Sol. Energy Mater. Sol. Cells*, 1994, **32**, 7-19.
10 S. C. Riha, D. C. Johnson and A. L. Prieto, *J. Am. Chem. Soc.*, 2011, **133**, 1383-1390.
11 Y. Xie, X. Zheng, X. Jiang, J. Lu and L. Zhu, *Inorg. Chem.*, 2001, **41**, 387-392.
12 A. Jagminas, R. Juškėnas, I. Gailiūtė, G. Statkutė and R. Tomašiūnas, *J. Cryst. Growth*, 2006, **294**, 343-348.
13 K.-H. Low, C.-H. Li, V. A. L. Roy, S. S.-Y. Chui, S. L.-F. Chan and C.-M. Che, *Chem. Sci.*, 2010, **1**, 515-518.
14 S. Deka, A. Genovese, Y. Zhang, K. Miszta, G. Bertoni, R. Krahne, C. Giannini and L. Manna, *J. Am. Chem. Soc.*, 2010, **132**, 8912-8914.
15 T. D. T. Ung and Q. L. Nguyen, *Nanosci. Nanotechnol.* , 2011, **2**, 6.
16 F. Scotognella, G. Della Valle, A. R. Srimath Kandada, D. Dorfs, M. Zavelani-Rossi, M. Conforti, K. Miszta, A. Comin, K. Korobchevskaya, G. Lanzani, L. Manna and F. Tassone, *Nano Lett.*, 2011, **11**, 4711-4717.
17 Y. Zhao, H. Pan, Y. Lou, X. Qiu, J. Zhu and C. Burda, *J. Am. Chem. Soc.*, 2009, **131**, 4253-4261.
18 A. Comin and L. Manna, *Chem. Soc. Rev.*, 2014, **43**, 3957-3975.
19 L. Zhang, C. Z. Huang, Y. F. Li and Q. Li, *Cryst. Growth Des.*, 2009, **9**, 3211-3217.
20 L. Zhang, S. J. Zhen, Y. Sang, J. Y. Li, Y. Wang, L. Zhan, L. Peng, J. Wang, Y. F. Li and C. Z. Huang, *Chem. Commun.*, 2010, **46**, 4303-4305.
21 Y. Liu and C. Z. Huang, *Nanoscale*, 2013, **5**, 7458-7466.
22 J. M. Luther, P. K. Jain, T. Ewers and A. P. Alivisatos, *Nat. Mater.*, 2011, **10**, 361-366.
23 Y. D. Zhu, J. Peng, L. P. Jiang and J. J. Zhu, *Analyst*, 2014, **139**, 649-655.
24 X. Liu, W.-C. Law, M. Jeon, X. Wang, M. Liu, C. Kim, P. N. Prasad and M. T. Swihart, *Adv. Healthcare. Mater.*, 2013, **2**, 952–957.
25 X. Liu, C. Lee, W. C. Law, D. Zhu, M. Liu, M. Jeon, J. Kim, P. N. Prasad, C. Kim and M. T. Swihart, *Nano Lett.*, 2013, **13**, 4333-4339.

26 C. M. Hessel, V. P. Pattani, M. Rasch, M. G. Panthani, B. Koo, J. W. Tunnell and B. A. Korgel, *Nano Lett.*, 2011, **11**, 2560-2566.
27 X. Liu, Q. Wang, C. Li, R. Zou, B. Li, G. Song, K. Xu, Y. Zheng and J. Hu, *Nanoscale*, 2014, **6**, 4361-4370.
28 Y. Zhao and C. Burda, *Energy Environ. Sci.*, 2012, **5**, 5564-5576.
29 P. Hu and Y. Cao, *J. Nanopar. Res.*, 2012, **14**, 1-8.
30 P. Huang, Y. Kong, Z. Li, F. Gao and D. Cui, *Nanoscale Res. Lett.*, 2010, **5**, 949-956.
31 X. Liu, X. Duan, P. Peng and W. Zheng, *Nanoscale*, 2011, **3**, 5090-5095.
32 X. Liu, X. Wang, B. Zhou, W.-C. Law, A. N. Cartwright and M. T. Swihart, *Adv. Funct. Mater.*, 2013, **23**, 1256-1264.
33 J. Zhu, Q. Li, L. Bai, Y. Sun, M. Zhou and Y. Xie, *Chem. Eur. J*, 2012, **18**, 13213-13221.
34 C. T. Campbell and C. H. F. Peden, *Science*, 2005, **309**, 713-714.
35 F. Cheng, T. Zhang, Y. Zhang, J. Du, X. Han and J. Chen, *Angew. Chem. Int. Ed.*, 2013, **52**, 2474-2477.
36 M. Nolan, S. C. Parker and G. W. Watson, *Surf. Sci.*, 2005, **595**, 223-232.
37 S. C. Riha, D. C. Johnson and A. L. Prieto, *J. Am. Chem. Soc.*, 2010, **133**, 1383-1390.
38 F. X. Rong, Y. Bai, T. F. Chen and W. J. Zheng, *Mater. Res. Bull.*, 2012, **47**, 92-95.
39 W. Chen, L. Hong, A.-L. Liu, J.-Q. Liu, X.-H. Lin and X.-H. Xia, *Talanta*, 2012, **99**, 643-648.
40 Q. Li, L. Zhang, J. Li and C. Lu, *TrAC-Trend Anal. Chem.*, 2011, **30**, 401-413.
41 S. Jiao, L. Xu, K. Jiang and D. Xu, *Adv. Mater.*, 2006, **18**, 1174-1177.
42 S.-Y. Zhang, C.-X. Fang, Y.-P. Tian, K.-R. Zhu, B.-K. Jin, Y.-H. Shen and J.-X. Yang, *Cryst. Growth Des.*, 2006, **6**, 2809-2813.
43 H. Cao, X. Qian, C. Wang, X. Ma, J. Yin and Z. Zhu, *J. Am. Chem. Soc.*, 2005, **127**, 16024-16025.
44 D. M. Wang, M. X. Gao, P. F. Gao, H. Yang and C. Z. Huang, *J. Phys. Chem. C*, 2013, **117**, 19219-19225.
45 Z. Lin, X. Dou, H. Li, Q. Chen and J.-M. Lin, *Microchim. Acta*, 2014, 1-7.
46 C. Xiao, Y. Zhang, A. Xie, Z. Wu, H. Wang and Y. Shen, *Materials Letters*, 2013, **111**, 51-54.
47 D. Dorfs, T. Härtling, K. Miszta, N. C. Bigall, M. R. Kim, A. Genovese, A. Falqui, M. Povia and L. Manna, *J. Am. Chem. Soc.*, 2011, **133**, 11175-11180.
48 E. J. Silvester, F. Grieser, B. A. Sexton and T. W. Healy, *Langmuir*, 1991, **7**, 2917-2922.
49 I. Kriegel, C. Y. Jiang, J. Rodriguez-Fernandez, R. D. Schaller, D. V. Talapin, E. da Como and J. Feldmann, *J. Am. Chem. Soc.*, 2012, **134**, 1583-1590.
50 Y. Bai, F. Rong, H. Wang, Y. Zhou, X. Xie and J. Teng, *J. Chem. Eng. Data*, 2011, **56**, 2563-2568.
51 M. Darouie, S. Afshar, K. Zare and M. Monajjemi, *J. Exp. Nanosci.*, 2012, **8**, 451-461.
52 P. K. Jain, X. Huang, I. H. El-Sayed and M. A. El-Sayed, *Acc. Chem. Res.*, 2008, **41**, 1578-1586.
53 J.-Z. Guo, H. Cui, W. Zhou and W. Wang, *J.Photoch. Photobio. A*, 2008, **193**, 89-96.
54 D. M. Wang, Y. Zhang, L. L. Zheng, X. X. Yang, Y. Wang and C. Z. Huang, *J. Phys. Chem. C*, 2012, **116**, 21622-21628.
55 S. Hanaoka, J.-M. Lin and M. Yamada, *Anal. Chim. Acta*, 2000, **409**, 65-73.